# The Figure-8 Magnetic Moment Coupling Potential and Valence Electron Kinetic Energy—A First-Order Criterion for Superconductivity

Zhaole Sun

Shenzhen Relativity Technology Co., Ltd., Shenzhen, Guangdong 518000

Email: e.mcc@163.com

## Abstract

Based on the Figure-8 electromagnetic standing wave plus eigen-drift electron model, this paper proposes a magnetic coupling pairing mechanism between Figure-8 magnetic moments and electron magnetic chains, and infers that the core condition for superconducting pairing is that the inter-electron magnetic coupling potential exceeds the sum of valence-electron kinetic energies., we derive the magnetic coupling potential energy between two electrons as $|U_m| \approx 14.57eV$ and define $\Gamma = 7.285eV$ as **a first-order criterion** for determining the superconducting capability of valence-shell electrons—that is, **the "golden threshold"** for superconductivity. Validated against NIST measured spectroscopic data for 28 ambient-pressure superconducting elemental solids, the overall relative offset between the average valence-electron kinetic energy and the golden boundary is $\delta = +0.52\%$ ; similarly, when using this golden threshold to evaluate good conductors such as Au, Ag, and Cu, the results are $\delta = -117.3\%$ , Significant difference. Thus, it can be concluded that this criterion possesses a high degree of scientific validity.It also indicates that whether an element exhibits superconducting properties is highly correlated with the kinetic energy of its outer valence electrons: the lower the kinetic energy, the more conducive it is to superconductivity; conversely, superconductivity is unlikely to occur. The principle behind this criterion is simple, and its physical picture is intuitive; it is expected to become a practical analytical tool for superconductivity research, providing both a new perspective for investigating the microscopic mechanisms of superconductivity and a theoretical reference for the screening and design of new superconducting materials.

**Keywords:** superconductivity; Figure-8 magnetic-moment electron magnetic chain; BCS Cooper pairs ; Eigen-Drift; first-order superconductivity criterion; valence electron kinetic energy; elemental superconductors

## 1.0 Introduction

Since its discovery, the microscopic mechanism of superconductivity has remained a central challenge in condensed matter physics. The BCS theory proposed by Bardeen, Cooper, and Schrieffer established the theoretical framework for conventional low-temperature superconductivity, positing that the formation of Cooper pairs via electro-acoustic coupling constitutes the microscopic basis of superconductivity [1].Building on this, McMillan developed a strong-coupling correction scheme, providing a semi-empirical estimate for the superconducting transition temperature in systems with strong electron-phonon coupling, thereby extending the applicability of the BCS theory [2]. However, this theoretical framework tends toward a post hoc explanation and struggles to provide a unified, a priori energy criterion for

determining whether an elemental material exhibits a tendency toward ambient-pressure superconductivity.

The discovery of high-temperature superconductivity in copper oxides shattered the temperature upper limit predicted by BCS theory and fully exposed the limitations of the electro-acoustic coupling model [3]. For high-temperature superconducting systems, Anderson proposed the Resonant Valence Bond (RVB) model, which offers a theoretical approach distinct from electro-acoustic coupling by focusing on spin pairing [4].Zhao Zhongxian's review systematically summarized research progress on high-temperature superconducting materials and physics, and identified the core, long-standing challenges in this field [5]. Although various theoretical frameworks have been developed, simple, computable criteria for predicting superconducting tendencies in elemental systems remain scarce.

This work is based on the previously proposed figure-8 electromagnetic standing wave plus intrinsic drift topological model of the electron [6]. Using valence-electron energy level data from the NIST measured spectral database [7], it attempts to establish a first-order criterion centered on valence-electron orbital kinetic energy. Validation and comparative analysis are carried out for elemental superconductors under ambient pressure. The validity and applicable boundary of this criterion for distinguishing superconducting and non-superconducting elements are discussed.

## 2.0 The Figure-8 Electromagnetic Standing Wave Model for Electrons

### 2.1 Introduction to the Electron Figure-8 Standing Wave Model

This paper adopts the "Figure-8 electromagnetic standing wave plus eigen-drift electron structure" model proposed in [6]. This model extracts only the core features directly related to Cooper pair formation; it rejects the point-particle assumption for electrons and describes electrons as a self-consistent, closed electromagnetic standing wave topological structure, in which the continuous figure-8 standing wave circulation within the wave is the source of the electron's spin properties;Since the figure-8 standing wave as a whole (Fig. 1a) undergoes eigen-drift within spherical space, the electronic surface of the spherical contour exhibits uniform electrical properties and is macroscopically non-magnetic (Fig. 1b). This chapter merely lays the groundwork for this electronic microstructure; the role of magnetic-axis coupling in the formation of Cooper-like pairs will be derived in detail later in the text.

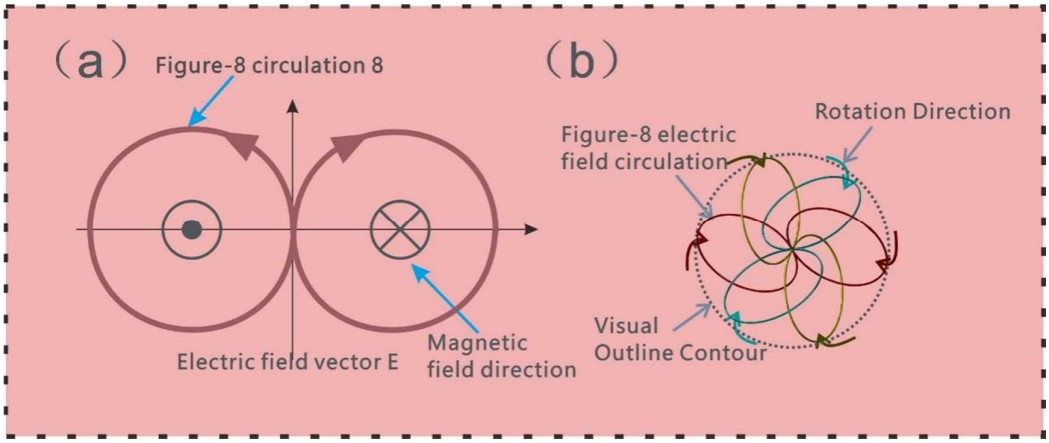



Fig. 1 Schematic snapshot of figure-8 electromagnetic standing wave circulation and eigen-drift

## 2.2 Mechanism of Formation of the Figure-8 Magnetic Moment Model

**Model state of electrons in the absence of an external field:** An figure-8 electromagnetic standing wave (Fig. 1a) contains a pair of oppositely oriented magnetic axes that are closed within the two loops; combined with the overall eigen-drift, this results in no directional deformation, a uniform negative electric field, and no net macroscopic magnetic response(Fig. 1b) .

**State of the electronic model under an external field:** When a uniform external magnetic field is applied, the magnetic axes within the standing wave couple with the external magnetic field via magnetic moment interaction. The originally spherically symmetric **figure-8 electromagnetic standing wave** structure undergoes oriented stretching and enters a state of **eigen-drift** collapse (Fig. 2a) :The standing wave is compressed perpendicular to the magnetic field and extends along the direction perpendicular to the magnetic field, transforming its spherical contour into an elongated, non-spherical boundary;The circulation streamlines within the standing wave are constricted by the magnetic field; the originally isotropically distributed bidirectional magnetic axes selectively align along the direction of the external field; the equivalent negative electron charges are rearranged in response to the deformation of the standing wave field, resulting in a gradient distribution of charge density along the outer contour: charge accumulates in regions perpendicular to the external magnetic field, while the charge density decreases significantly along the direction of the magnetic axes.The electrostatic repulsion along the magnetic axes weakens, providing favorable conditions for the mutual coupling of the magnetic axes.

**Simplified electron magnetic moment model:** To more vividly describe the mechanism of electron action in the superconducting process, the most prominent features of electrons are represented using a simple graphical symbol (Fig. 2b), forming an engineered simplified equivalent model. Internal dense streamlines are omitted, retaining only the deformed contour, paired magnetic axes, and boundary negative charge markers to intuitively illustrate the structural collapse induced by the external magnetic field.For consistency throughout the text, this simplified model will hereafter **be referred to as the "figure-8 magnetic moment**."

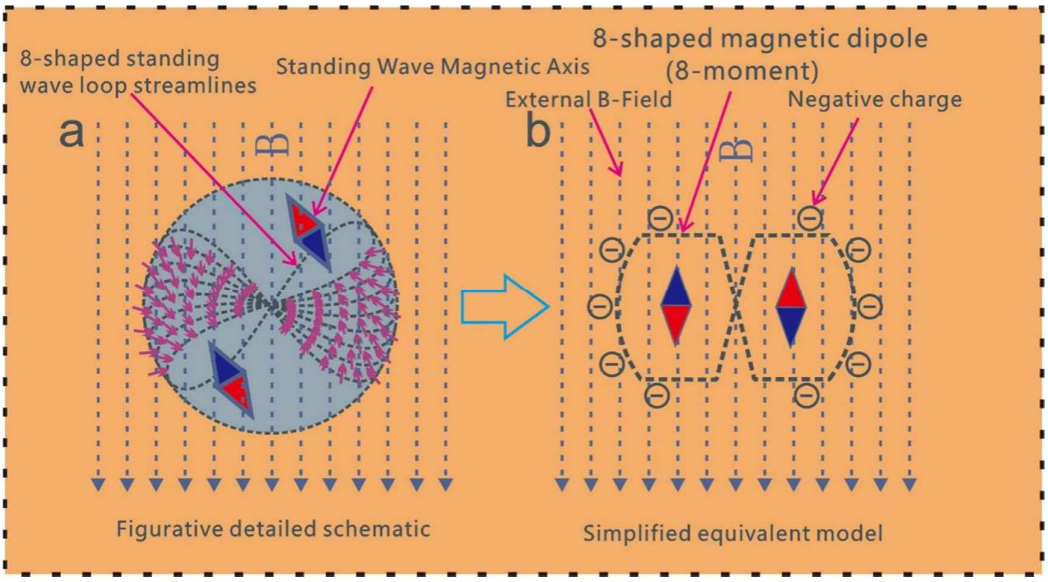



Fig. 2 Schematic diagram of the eigen-drift collapse of an electron figure-8 standing wave forming a figure-8 magnetic moment under an external magnetic field

### 2.3 Mechanism of Electron Magnetic Flux Formation

Based on **the figure-8 magnetic moment** model established under the aforementioned external field, the two major electrical properties of the **figure-8 magnetic moment** provide favorable conditions for the smooth coupling of multiple figure-8 magnetic moments. Adjacent **figure-8 magnetic moments** generate complementary attraction between oppositely charged magnetic axes, reducing the strength of the electrostatic field at the adjacent contact surfaces,and the electrostatic repulsion is weakened. Consequently**, the figure-8 magnetic moments** at this point can successfully pair to form **electron elementary pairs** with a Cooper-pair-like structure **.** When numerous **electron figure-8 magnetic moments** are connected in sequence, they form an electron elementary magnetic chain resembling a long chain. This structure is termed **the electron magnetic chain** (Fig. 3).

**The coupling of electronic magnetic chains with Cooper pairs is more scientifically sound:**

The physical model in which Cooper pairs rely on phonons for pairing has obvious limitations: the attractive force is weak and lagging, there is no stable real-space bound structure, and the explanation for the pairing mechanism is insufficient.

**Instantaneous Dissociation Between Electronic and Magnetic Flux Lines :**Since the magnetism at both ends of **the figure-8 magnetic moment** is generated by internal figure-8 electromagnetic standing-wave currents, the magnetic polarity intensity on both sides varies with the frequency of the electromagnetic standing wave$\boldsymbol{f = 1.236 \times 10^{20}\ Hz}$ . Because this value is very high, whenever the internal standing wave **of a figure-8 magnetic moment** approaches zero, the **two** adjacent **figure-8 magnetic moments** experience a momentary loss of magnetism, leading to instantaneous dissociation between electron magnetic fluxes (Fig. 3) .

**Prerequisites for the formation of the electron magnetic flux:**

**Ultra-low temperature:** The kinetic energy of valence electron thermal motion is significantly reduced, and thermal perturbations that interfere with the eigen-drift of the internal figure-8 standing waves of electrons are greatly suppressed; the orientation of valence electron magnetic moments is no longer randomly disrupted by thermal motion, and the magnetic coupling dissociation region remains stable.When the potential energy of the valence electron magnetic coupling exceeds the total kinetic energy of the two electrons—satisfying the first-order superconductivity criterion proposed in this paper—adjacent electrons' figure-8 magnetic moments pair via opposite-pole magnetic attraction, offsetting the inter-electron Coulomb repulsion. A large number of electrons then arrange themselves in an ordered series, forming a continuous magnetic chain system with global phase locking, which provides the microscopic structural basis for macroscopic superconducting effects such as zero resistance and Meissner-type diamagnetism.

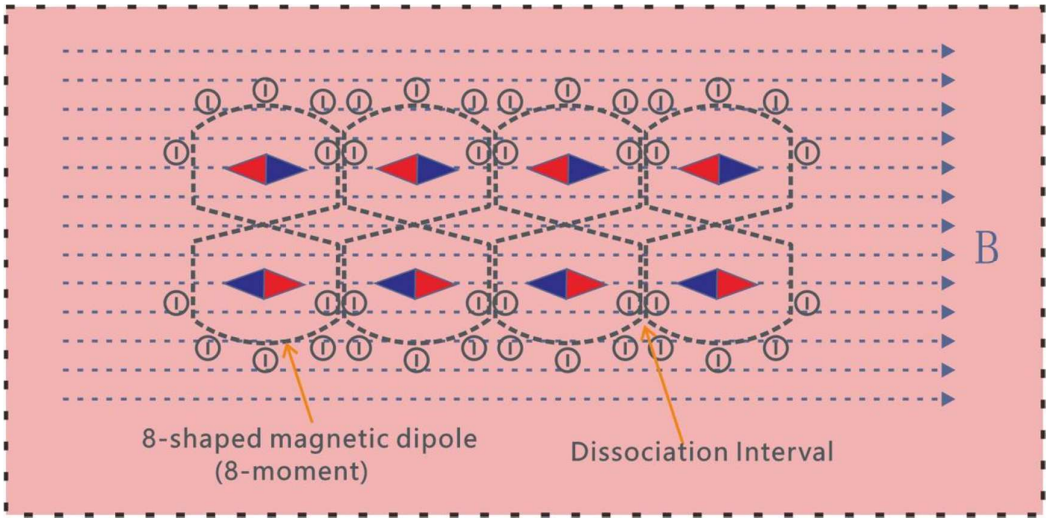



Fig. 3 Mechanism of Electron Magnetic Chain Formation Under External Magnetic Fields

**External Field Induction:** An external magnetic field can impose directional constraints on the internal figure-8 standing-wave drift trajectories of electrons, unifying the orientation of all electron magnetic dipoles. This promotes the spontaneous pairing of adjacent electrons' figure-8 magnetic moments via opposite-pole alignment, effectively suppressing the Coulombic electrostatic repulsion between electrons and establishing an ordered foundation for long-range, coherent electron magnetic chains.Without the orienting effect of an external field, electron magnetic moments are arranged randomly and disorderly, significantly reducing the probability of pairing that satisfies the energy criteria for magnetic moment coupling, making it difficult to form a globally coherent magnetic chain structure.

**Effect of the self-induced magnetic field generated by electric current:**Carrier transport in a conductor excites a closed-loop self-induced magnetic field in the cross-section perpendicular to the current. At any point in the conductor, the direction of this field aligns with the tangent to the circumferential magnetic dipole attraction at

that point. Acting parallel to nearby valence electrons, it induces the orientation and alignment of figure-8 magnetic moments (Fig. 4), thereby enabling the ordered pairing of figure-8 magnetic moments without the need for an external magnetic field. The self-induced magnetic field synchronously constrains the orientation of all figure-8 magnetic moments along the current path, driving complementary coupling between adjacent units with opposite poles. These units connect in series within the cross-section perpendicular to the current, forming a closed-loop electronic magnetic flux (Fig. 4);This microscopic mechanism explains the intrinsic reason why an electrified superconducting circuit can stably maintain a zero-resistance superconducting state without an external field, and it is the core condition for self-driven carrier pairing. This self-field coupling effect causes a current gradient distribution in the superconducting conductor, which differs from the skin effect in conventional conductors caused by alternating eddy currents; the underlying physical mechanisms of the two are entirely different.

**Inertial Mechanism of Superconductivity:** The mechanism maintaining superconducting current flow is consistent with Newton's classical law of inertia. The initial external power source serves only to initiate the process, driving the valence electrons into directed motion, forming an ordered figure-8 magnetic moment flux chain, and establishing a stable velocity. After the power source is removed, there is no scattering resistance within the superconducting system; the electron flux chain follows the law of inertia to maintain its original state of motion, which manifests macroscopically as the continued presence of superconducting current.

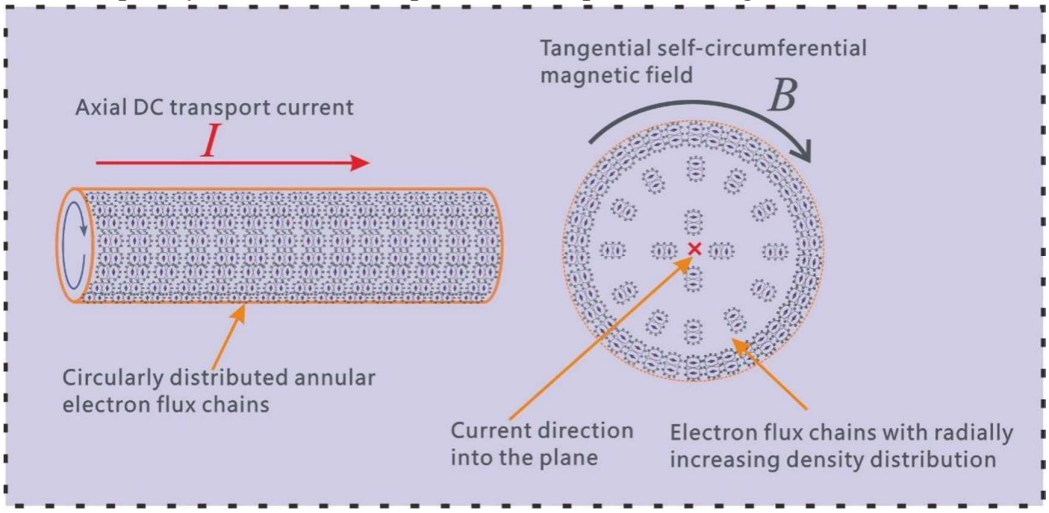



Fig. 4 Schematic of the cross-sectional and circumferential distribution of electron flux chains within cylindrical DC superconductors

## 3.0 Derivation of the Mechanism of Electron-Magnetic Coupling and Dynamics in Superconductors

### 3.1 Mechanisms of Inter-electron Interactions Within Superconductors

**Model Approximations and Boundary Conditions:** The preceding discussion of the formation mechanism of electron magnetic flux chains was limited to a single-electron perspective; however, within the superconducting solid, the interacting factors are highly complex.At this stage, this model retains only the dominant

physical terms: the attractive potential due to the coupling of magnetic moments in two-electron loop currents ($U_m(r)$), the kinetic energy of valence-shell electrons in their eigenorbits ($E_{ks}$), and the thermal excitation energy ($2k_BT$ ); since the magnetic axes of the electron magnetic moments are perpendicular to the electric field direction, secondary factors such as Coulomb repulsion, collective phase coherence effects among multiple electrons, orbital overlap modulation, and lattice perturbations are temporarily neglected.

**Kinetic energy of valence-shell electrons and free conduction electrons:** In this study, it is defined that $E_{ks}$ represents the intrinsic kinetic energy of valence-shell electrons bound to the atomic orbitals of an isolated atom; $E_{kf}$ represents the intrinsic kinetic energy of free conduction electrons that have escaped the localized binding of the atomic nucleus after the solid has formed. The valence-shell s electrons of an isolated atom are bound by the atomic nuclear potential, and their intrinsic kinetic energy $E_{ks}$ is relatively low; after atoms aggregate to form a solid, the valence electrons transform into free conduction electrons, and the corresponding intrinsic kinetic energy $E_{kf}$ is slightly greater than the kinetic energy $E_{ks}$ of the valence-shell electrons in an isolated atom.

**Necessary condition for superconducting pairing:** The magnetic coupling potential energy of the two electrons competes with their total kinetic energy, establishing the fundamental physical picture and qualitative criteria for superconducting pairing. In a two-electron system, the magnetic coupling attractive potential energy being greater than the total kinetic energy of the electrons is a necessary, but not sufficient, condition for pairing.

$$|\boldsymbol{U_m(r)}| > \boldsymbol{2k_BT + 2E_{kf}} \quad \textbf{(1)}$$

$E_{ks}$ Derived from ionization energies measured in experiments on isolated atoms; $E_{kf}$ is the kinetic energy parameter for free electrons in solids introduced in this model. Since no direct experimental measurements are currently available, this paper assumes that the numerical deviation between the two is small; therefore, the above equation is transformed as follows:

$$|\boldsymbol{U_m(r)}| > \boldsymbol{2k_BT + 2(E_{ks} + \Delta E_k)} \quad \textbf{(2)}$$

$\Delta E_k$ : When atoms condense to form a solid, the increment in kinetic energy of free electrons resulting from the conversion of orbital kinetic energy is generally given by $\boldsymbol{\Delta E_k > 0}$ .

**Scope of application of this model:** It is used solely for the qualitative assessment of an element's superconducting tendency, to explain superconducting differences among orbital systems in different valence shells, and to establish fundamental correlations between electron kinetic energy thresholds and superconducting phase transitions. Subsequent research will build upon this initial framework to gradually introduce macroscopic coherence order parameters, orbital configuration corrections, and multi-electron coupling terms, thereby constructing a complete system of dynamical equations capable of accurately describing superconducting phase transitions.

### 3. 2 Derivation of the Attractive Potential for Inter-electron Magnetic Coupling

Based on the results of my previous research and relevant existing theoretical data, the following physical constraints and symbolic expressions have been identified:

Results from my previous research [6]:

**Electron radius:** $\boldsymbol{r_e = \frac{\hbar}{m_e c} = 3.86 \times 10^{-13}\ m}$

**Equivalent electron radius:** $\boldsymbol{R_e = 2r_e}$

**Standing wave frequency of the electron:** $\boldsymbol{f_e = \frac{c}{\lambda} = \frac{c}{2\pi r_e} \approx 1.236 \times 10^{20}\ Hz}$

**Electron spin magnetic moment:** $\boldsymbol{\mu_e = \mathrm{g} \cdot \frac{e}{2m_e} \cdot \frac{\hbar}{2} = g \cdot \frac{e\hbar}{4m_e}}$

**Existing physical data:**

$e$ where e is the elementary charge, $\varepsilon_0$ is the permittivity of free space, and $\mu_0$ is the magnetic permeability of free space;

$k_B$ the Boltzmann constant, and $T$ is the thermodynamic temperature;

$U_m$ is the potential energy of the magnetic dipole interaction;

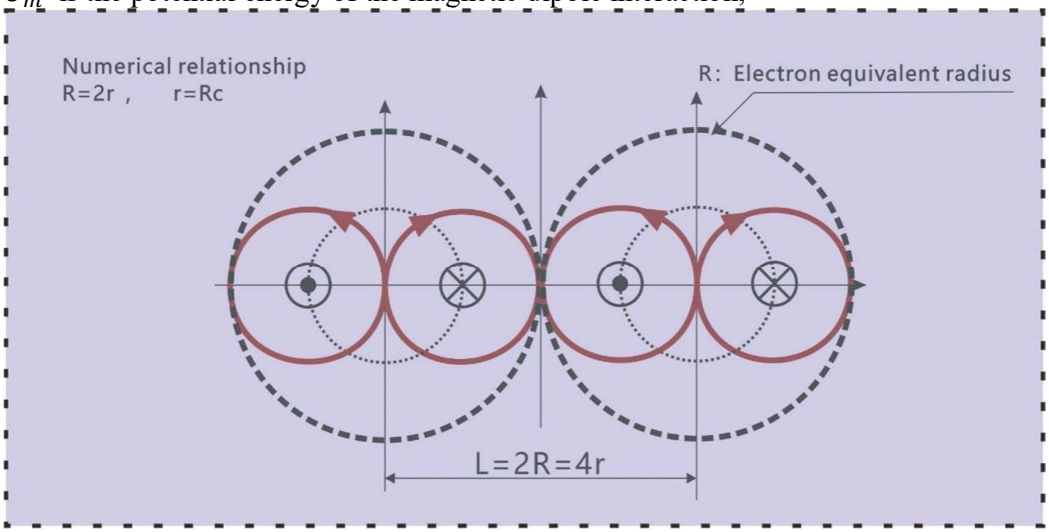



Fig. 5 Schematic of the positional relationship between two approaching figure-8 standing-wave electrons

**Magnetic coupling attraction potential between the circular magnetic moments on the edges of the two electrons as they approach**:

$$|\boldsymbol{U_m(r)}| = \frac{\boldsymbol{\mu_0}}{\boldsymbol{4\pi}} \cdot \frac{\boldsymbol{\mu_1 \cdot \mu_2}}{\boldsymbol{r^3}} \tag{3}$$

The conduction electron structure within the system is identical, and the magnetic moments of adjacent electrons are equal: $u_1 = u_2 = u_e$ . When two adjacent electrons approach each other, their center-to-center distance is $\boldsymbol{2R_e}$ (Fig. 5), which simplifies to:

$$|\boldsymbol{U_m(r)}| = \frac{\boldsymbol{\mu_0 \mu_e{}^2}}{\boldsymbol{4\pi(2r_e)^3}} = \frac{\boldsymbol{\mu_0}}{\boldsymbol{4\pi}} \cdot \frac{\boldsymbol{(ge\hbar)^2}}{\boldsymbol{16m_e^2}} \cdot \left(\frac{\boldsymbol{m_e c}}{\boldsymbol{4\hbar}}\right)^3 \tag{4}$$

$$|\boldsymbol{U_m(r)}| = \frac{\boldsymbol{\mu_0 m_e c^3 (ge)^2}}{\boldsymbol{4096\pi\hbar}} \tag{5}$$

Substituting all parameters yields:

$$|U_m(r)| = 2.33375 \times 10^{-18}\ \text{J} \tag{6}$$

Since $1\ \text{eV} = 1.602 \times 10^{-19}\ \text{J}$ , the above values can be converted to electronvolts:

$$|U_m(r)| = \frac{2.33375 \times 10^{-18}}{1.602 \times 10^{-19}} \approx 14.57\ \text{eV} \tag{7}$$

This value shows that the magnetic potential energy is close to the orbital kinetic energy of the outermost electrons of an atom. Below, we will conduct a more in-depth analysis of this data in relation to the kinetic energy of the outermost valence electrons in superconducting materials.

### 3.3 Analysis of the Total Kinetic Energy of Free Electrons in Superconducting Elements

Within the framework of this model, we adopt the approximation that the first ionization energy is equivalent to the orbital kinetic energy of the outermost valence electrons: $E_{ks}$ . The first ionization energy is defined as the minimum energy required to remove a valence electron from a neutral, isolated atom; according to the Virial Theorem [8], in a Coulomb-bound system, the total energy of an electron equals the negative of its orbital kinetic energy. Therefore, the orbital kinetic energy of the valence electrons is numerically equal to the first ionization energy.This approximation applies only to the valence electrons of isolated atoms in their ground state and serves as a preliminary simplifying assumption for establishing the superconducting screening criterion in this paper; it does not account for factors such as the solid-state lattice field or electron correlations.

Table 1: Comparison Table of Orbital Kinetic Energy of Valence Shells in Normal-Pressure Superconducting Elements and First-Order Criteria (Raw ionization energy data [7]: NIST Atomic Spectra Database)

| No. | Element symbol | Valence configuration | $E_{ks}$ (eV) | $\Gamma$ (eV | $\Delta E_k + k_B T$ | $T_c$ (K) |
|---|---|---|---|---|---|---|
| 1 | Be | [He]2s² | 9.323 | 7.285 | -2.038 | 0.026 |
| 2 | Al | [Ne]3s²3p¹ | 5.986 | 7.285 | +1.299 | 1.18 |
| 3 | Ti | [Ar]3d²4s² | 6.828 | 7.285 | +0.457 | 0.40 |
| 4 | V | [Ar]3d³4s² | 6.746 | 7.285 | +0.539 | 5.30 |
| 5 | Zn | [Ar]3d¹⁰4s² | 9.394 | 7.285 | -2.109 | 0.85 |
| 6 | Ga | [Ar]3d¹⁰4s²4p¹ | 5.999 | 7.285 | +1.286 | 1.08 |
| 7 | Zr | [Kr]4d²5s² | 6.634 | 7.285 | +0.651 | 0.61 |
| 8 | Nb | [Kr]4d⁴5s¹ | 6.759 | 7.285 | +0.526 | 9.25 |
| 9 | Mo | [Kr]4d⁵5s¹ | 7.092 | 7.285 | +0.193 | 0.92 |
| 10 | Tc | [Kr]4d⁵5s² | 7.280 | 7.285 | +0.005 | 7.80 |
| 11 | Ru | [Kr]4d⁷5s¹ | 7.361 | 7.285 | +0.076 | 0.49 |
| 12 | Cd | [Kr]4d¹⁰5s² | 8.994 | 7.285 | -1.709 | 0.52 |
| 13 | In | [Kr]4d¹⁰5s²5p¹ | 5.786 | 7.285 | +1.499 | 3.41 |
| 14 | Sn | [Kr]4d¹⁰5s²5p² | 7.344 | 7.285 | -0.059 | 3.72 |
| 15 | La | [Xe]5d¹6s² | 5.577 | 7.285 | +1.708 | 4.90 |

| | | | | | | |
|---|---|---|---|---|---|---|
| 16 | Hf | [Xe]4f$^{14}$5d$^{2}$6s$^{2}$ | 6.825 | 7.285 | +0.460 | 0.13 |
| 17 | Ta | [Xe]4f$^{14}$5d$^{3}$6s$^{2}$ | 7.550 | 7.285 | -0.265 | 4.48 |
| 18 | W | [Xe]4f$^{14}$5d$^{4}$6s$^{2}$ | 7.864 | 7.285 | -0.679 | 0.015 |
| 19 | Re | [Xe]4f$^{14}$5d$^{5}$6s$^{2}$ | 7.834 | 7.285 | -0.549 | 1.70 |
| 20 | Os | [Xe]4f$^{14}$5d$^{6}$6s$^{2}$ | 8.438 | 7.285 | -1.153 | 0.66 |
| 21 | Ir | [Xe]4f$^{14}$5d$^{7}$6s$^{2}$ | 8.967 | 7.285 | -1.682 | 0.11 |
| 22 | Hg | [Xe]4f$^{14}$5d$^{10}$6s$^{2}$ | 10.438 | 7.285 | -3.153 | 4.15 |
| 23 | Tl | [Xe]4f$^{14}$5d$^{10}$6s$^{2}$6p$^{1}$ | 6.108 | 7.285 | +1.177 | 2.39 |
| 24 | Pb | [Xe]4f$^{14}$5d$^{10}$6s$^{2}$6p$^{2}$ | 7.417 | 7.285 | -0.132 | 7.19 |
| 25 | Th | [Rn]6d$^{2}$7s$^{2}$ | 6.307 | 7.285 | +0.978 | 1.37 |
| 26 | Pa | [Rn]5f$^{2}$6d$^{1}$7s$^{2}$ | 5.89* | 7.285 | +1.395 | 1.40 |
| 27 | U | [Rn]5f$^{3}$6d$^{1}$7s$^{2}$ | 6.194 | 7.285 | +1.091 | 0.20 |
| 28 | Am | [Rn]5f7s$^{2}$ | 5.974 | 7.285 | +1.311 | 0.60 |
| — | — | — | $\overline{E_{ks}}$ =7.247 eV | — | — | — |

Table 2: Validation Table: Valence-Shell Intrinsic Orbital Kinetic Energy & First-Order Criterion for Elements without Ambient-Pressure Superconductivity (Raw ionization data [7]: NIST Atomic Spectra Database)

| No. | Element symbol | Valence configuration | $E_{ks}$ (eV) | $\Gamma$ (eV) | $\Delta E_k + k_B T$ | $T_c$ (K) |
|---|---|---|---|---|---|---|
| 1 | Cu | [Ar]3d$^{10}$4s$^{1}$ | 15.453 | 7.285 | 8.168 | — |
| 2 | Ag | [Kr]4d$^{10}$5s$^{1}$ | 15.152 | 7.285 | 7.867 | — |
| 3 | Au | [Xe]4f$^{14}$5d$^{10}$6s$^{1}$ | 18.451 | 7.285 | 11.166 | — |
| 4 | Ni | [Ar]3d$^{8}$4s$^{2}$ | 15.28 | 7.285 | 7.995 | — |
| 5 | Co | [Ar]3d$^{7}$4s$^{2}$ | 15.762 | 7.285 | 8.477 | — |
| 6 | Mn | [Ar]3d$^{5}$4s$^{2}$ | 14.868 | 7.285 | 7.583 | — |
| — | — | — | $\overline{E_{ks}}$ = 15.828 eV | — | — | — |

Note: The orbital kinetic energy of valence electrons is approximated by the first ionization energy, ignoring corrections from the solid lattice field. $\Gamma$: golden threshold; $E_{ks}$, $\Delta E = \Delta E_k + k_B T$ : defined in the preceding text.

Since the interior of a superconductor consists entirely of collisions between two electrons and magnetic coupling, the potential energy of the magnetic coupling is greater than the sum of the kinetic energies of the two electrons. Therefore, the following relationship can be established:

$$|U_m(r)| > 2k_B T + 2(E_{ks} + \Delta E_k) \quad (8)$$

Given that $E_{ks}$ , the above equation can be rearranged to derive the criterion for determining the superconducting critical temperature:

$$2\Delta E_k + 2k_B T = |U_m(r)| - 2E_{ks} \quad (9)$$

Simplify:

$$\boldsymbol{\Delta E_k + k_B T = \frac{|U_m(r)|}{2} - E_{ks}} \quad \textbf{(10)}$$

where $|U_m| \approx 14.57eV$ is the fixed threshold for the magnetic coupling potential energy of the two-electron circulating current; let:

$$\boldsymbol{\Gamma = \frac{|U_m(r)|}{2} = 7.285eV} \quad \textbf{(11)}$$

$\boldsymbol{E_{ks}}$ To transfer the intrinsic kinetic energy of electrons to the valence band, where $k_B$ is the Boltzmann constant**.** For a comprehensive analysis, we first sum the orbital kinetic energies of the 28 elements in Table 1 and calculate the average: $\boldsymbol{\overline{E_{ks}}}$ **= 7.247 eV.** Substituting this value into the above equation**,** $\boldsymbol{E_{ks}}$ **:**

$$\boldsymbol{\Delta E_k + k_B T = \Gamma - 7.247 = 7.285 - 7.247 = 0.038\ eV} \quad \textbf{(12)}$$

To quantitatively compare the degree of agreement between the kinetic energy of the valence electron orbitals and the attractive potential of the interelectron magnetic coupling, we specifically define **the relative offset of the superconductivity criterion** as $\boldsymbol{\delta}$ **:**

$$\boldsymbol{\delta = \frac{\Delta E_k + k_B T}{|U_m(r)|} = \frac{\Gamma - \overline{E_{ks}}}{2\Gamma}} \quad \textbf{(13)}$$

From this, we obtain **the** overall average **relative offset for** ambient-pressure superconductivity $\boldsymbol{\delta}$ :

$$\boldsymbol{\delta = \frac{0.038}{7.285} \approx +0.52\%} \quad \textbf{(14)}$$

**This result intuitively demonstrates that the accuracy of the golden threshold in the statistics of ambient-pressure superconductivity is:** $\boldsymbol{0.52\%}$ **, which is extremely small.** $\boldsymbol{\Gamma = 7.285eV}$ Thus, **this** appears to be **the golden threshold** for distinguishing **superconductivity**.

### 3.4 Case Study of Negative Control Samples

To further substantiate the validity of the above criterion, we analyzed elements that are non-superconducting at ambient pressure and are typical good conductors. According to (Table 2), the average of the orbital kinetic energies of these six elements is: $\boldsymbol{\overline{E_{ks}}}$ **= 15.828 eV.** Substituting this value for $\boldsymbol{E_{ks}}$ into **(12):**

$$\boldsymbol{\Delta E_k + k_B T = \Gamma - 15.828 = 7.285 - 15.828 = -8.543} \quad \textbf{(15)}$$

This yields **the** overall average **relative offset** $\boldsymbol{\delta}$ for non-superconducting elements at ambient pressure:

$$\boldsymbol{\delta = \frac{-8.543}{7.285} \approx -117.3\%} \quad \textbf{(16)}$$

It is evident that the average kinetic energy of the negative samples differs significantly from the pairing critical threshold, with a deviation of 117.3%. The energy conditions do not satisfy the requirements for magnetic coupling pairing at all,

which quantitatively explains why superconducting electron pairs cannot form in the bulk of this group of elements at ambient pressure—a finding consistent with experimental observations.

**A counterintuitive fact: room-temperature good conductors have no connection to superconductivity.**

Cu, Ag, and Au are highly conductive noble metals with 4s/5s/6s valence electrons in their valence shells, exhibiting excellent direct-current conductivity; however, a superconducting phase transition has never been observed in their bulk forms at ambient pressure—a classic problem that traditional BCS theory struggles to explain quantitatively.BCS theory simply attributes this phenomenon to weak electro-acoustic coupling, offering only a qualitative description and lacking a unified energy threshold to distinguish between superconducting and non-superconducting elements.Within the framework of this model, although all three elements possess outer-shell s valence electrons, the kinetic energy of their valence electrons is relatively high. The attractive potential of the magnetic coupling between electrons is insufficient to counteract the kinetic energy of the valence electrons themselves; consequently, the figure-8 magnetic moments and electron magnetic flux cannot form stable bound pairs, and thus these elements do not exhibit a tendency toward superconductivity at ambient pressure.

Ni, Co, and Mn are all non-superconducting metals at ambient pressure; their valence electron configurations include unfilled 3d orbitals, and spontaneous magnetic order exists within the system. Magnetic order disrupts the quantum coherence of electron pairing; combined with the fact that their valence electron kinetic energy exceeds the threshold value of the criterion, these dual mechanisms collectively suppress the occurrence of a superconducting phase transition.

**Conclusion:** $\boldsymbol{\Gamma = 7.285}$ eV represents the "golden threshold" for determining whether an elemental metal possesses superconducting tendencies; $\boldsymbol{E_{ks} < \Gamma}$ indicates that the material meets the preliminary physical conditions for superconductivity, while $\boldsymbol{E_{ks} > \Gamma}$ generally indicates that the material does not meet these conditions—the greater the deviation, the lower the likelihood of superconductivity. The statistical comparison results between the two sets of samples are shown in (Table 3):

**Table 3** Comparison of Criteria Between Ambient-Pressure Superconducting Samples and Ambient-Pressure Non-Superconducting Good Conductor Samples

| **Ambient-pressure elemental sample** | **N** | $\boldsymbol{\overline{E_{ks}}}$ **(eV)** | $\boldsymbol{\Gamma}$ **(eV)** | $\boldsymbol{\delta}$ | **Status** |
|---|---|---|---|---|---|
| **SC elements** | 28 | 7.247 | 7.285 | +0.52% | Satisfied |
| **Non-SC conductors** | 6 | 15.828 | 7.285 | −117.3% | Not satisfied |

Note: N, sample count; $\boldsymbol{\overline{E_{ks}}}$ **,** mean kinetic energy of valence electrons; $\boldsymbol{\Gamma}$ **,** golden threshold; $\boldsymbol{\delta}$**,** relative deviation. SC, superconducting; Non-SC, non-superconducting.

# 4.0 Discussion

## 4.1 The " $\Gamma = 7.285$ eV " Is Merely a First-Order Criterion

In this paper, using the Virial Theorem, the first ionization energy is equated to the kinetic energy of the valence electron orbital: for a Coulomb-bound atomic state, the average kinetic energy of the electron is numerically equal to the ionization energy. It should be noted that this value is derived from spectral measurements of isolated atoms;when atoms aggregate to form a solid-state lattice, valence electrons are modulated by the lattice potential, causing a shift in orbital kinetic energy; therefore, this threshold is used only as a first-order criterion. This criterion is a necessary but not sufficient condition; it does not follow that the lower the kinetic energy, the higher the critical temperature $T_c$ . Superconducting elements with high $T_c$ tend to be distributed within a window around this threshold;The data cannot be fully reconciled; if a perfect match were achieved, it would lead to the conclusion of room-temperature superconductivity, which contradicts existing experimental evidence. At this stage, this criterion is used only for a first-order preliminary assessment of elemental superconductors; factors such as crystal structure, orbital hybridization, and lattice vibrations further modulate the critical temperature and have not yet been incorporated into the quantitative equation.

## 4.2 Comparison of This Model with BCS Theory

The BCS theory is a semi-quantitative theory; its critical temperature expression relies on fitting coupling parameters and has limited predictive power for elemental superconductivity. This model constructs a first-order criterion based on the balance between the coupling potential energy of electron magnetic moments and the kinetic energy of valence electrons. The core physical quantities are supported by both mathematically derivable and experimentally measurable data, and there are distinct differences in the underlying physical picture between the two theories.

## 4.3 Precise Measurement of Valence Electron Kinetic Energy Will Become a Research Focus

Various experimental techniques are currently available to probe the momentum and kinetic energy of valence electrons within a crystal: Compton profile spectroscopy can obtain the bulk valence electron momentum distribution, from which the average kinetic energy is derived through integration; angle-resolved photoemission spectroscopy (ARPES) can characterize the energy band dispersion of surface electrons at high resolution; and (e,2e) electron momentum spectroscopy can directly measure single-electron momentum information. However, few existing experiments have specifically targeted superconducting elements to quantitatively compare the differences in valence electron kinetic energy between the normal and superconducting states near the critical temperature. Therefore, the precise measurement of valence electron kinetic energy within the crystal is a key experimental direction for verifying the magnetic coupling pairing criterion proposed in this paper and advancing research into the mechanisms of superconductivity.

# 5.0 DC Self-Field Current Gradient Distribution in Superconducting Conductors

## 5.1 Experimental Objectives and Theoretical Basis

The classical homogeneous current-carrying superconductor model assumes a uniform current density, with the internal magnetic field satisfying $B(r) \propto r$ . Under the electron magnetic flux model presented in this paper, the self-induced magnetic field causes the figure-8 magnetic moments to couple in an ordered manner, causing the current to accumulate at the surface and the current density to increase linearly in the radial direction $J(r) = Ar$ . It is derived that the internal magnetic field satisfies $B(r) \propto r^2$ , forming an observable distinction from the classical model.This experiment tests the model's predictions regarding the current gradient distribution by measuring the radial distribution of the internal magnetic field within a superconducting cylinder.

## 5.2 Derivation and Prediction of the Magnetic Field Distribution

**Under direct current (DC), superconducting conductors exhibit a gradient distribution effect:** influenced by the radial magnetic field gradient, a superconducting cylinder displays a distinct radial current gradient distribution in a steady-state DC condition. According to the model derivation, when a DC current is applied to a superconductor, the magnetic field strength at different radial positions (Fig. 6) satisfies the following relationships: $\frac{B_2}{B_1} = \frac{R_2^2}{R_1^2}$ **and** $\frac{B_3}{B_1} = \frac{R_3^2}{R_1^2}$ . The derivation of these relationships is presented below.

**Specimen Geometric Model:** The specimen is a grain-boundary-free, single-crystal, solid superconducting cylinder with a radius of $R3$ . The radii of the bottom of the outer measurement holes from the centerline are $R1$、$R2$, :

$$R_1 = 5\ mm\ , R_2 = 7.07\ mm\ , R_3 = 10\ mm$$

A constant direct current is applied: $I$ ; at the center: $r = 0$ ; on the outer wall: $r = R$ .

**Assumptions regarding the current distribution:** It is assumed that the internal current density increases linearly along the radial direction:

$J(r) = Ar$

$A$ It is constant, with the current density increasing as one approaches the outer wall.

**Theoretical Derivation:**

Enclosed current within a radius of $r$ :

$$\boldsymbol{I_{enc}(r) = \int_0^r Ar' \cdot 2\pi r' dr' = \frac{2\pi A}{3} r^3} \quad \textbf{(17)}$$

Internal magnetic field (Ampère's circuital law):

$$\boldsymbol{B(r) = \frac{\mu_0 I_{enc}(r)}{2\pi r} = \frac{\mu_0 A}{3} r^2} \quad \textbf{(18)}$$

The internal magnetic field is proportional to the square of the radial coordinate: $B(r) \propto r^2$ .

Theoretical proportionality prediction:

Based on the aforementioned conditions, the relationship between the radial radius of the superconductor's cross-section and the radial electric field can be derived:

$$\boldsymbol{\frac{B_2}{B_1} = \frac{R_2^2}{R_1^2} = 2 \quad \frac{B_3}{B_1} = \frac{R_3^2}{R_1^2} = 4} \quad \textbf{(19)}$$

This quadratic proportionality can be verified simply by measuring the relative ratios of the magnetic fields at three locations inside the conductor, thereby validating the electronic magnetic flux model of DC gradient stratification.

### 5.3 Experimental Protocol and Evaluation Criteria

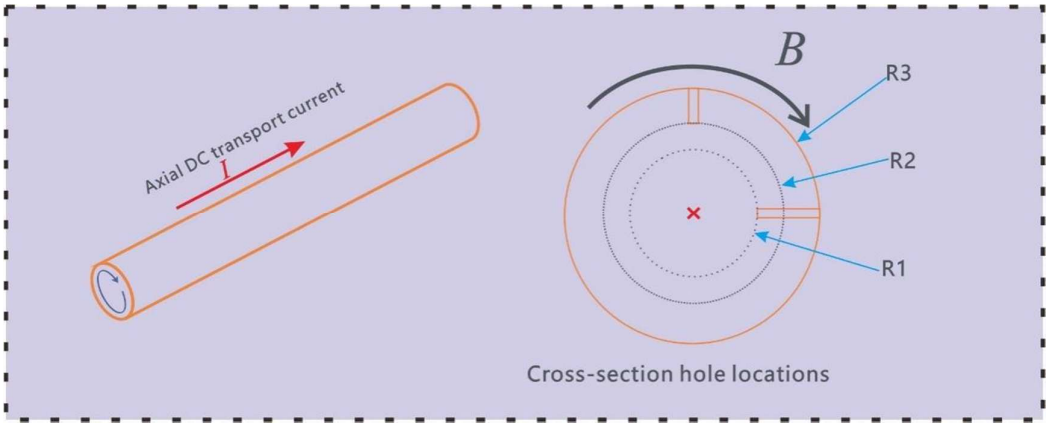



Fig. 6 Cylindrical superconducting specimen. Holes arranged at three different radial layers are used to measure the circumferential magnetic field for verification.

The specimen is a grain-free single-crystal superconducting cylinder with microholes drilled radially along its sidewall to allow Hall probes to penetrate the interior and measure the tangential magnetic field. Experimental procedure: The specimen is cooled to the superconducting state, and a constant direct current below the critical current is applied; nano-Hall probes are sequentially placed at three radial measurement points to collect magnetic field data; the measured magnetic field ratios are calculated and compared with theoretical predictions.

Conclusion: If the measured ratios are close to 2 and 4, this supports the current stratification hypothesis of this model; if there is a significant deviation, it indicates that the radial linear current-carrying hypothesis does not hold, and the model requires revision. Measurements are repeated multiple times to suppress errors caused by positioning and current fluctuations.

### 5.4 Analysis of Experimental Feasibility

Using a cryogenic vacuum sample stage, non-contact nano-Hall probes, and a low-ripple DC power source, it is possible to perform precise, point-by-point detection of the internal magnetic field in superconductors. This approach provides an independent experimental verification method for the electronic magnetic flux model presented in this paper.

---

## 6.0 Conclusions

**Based on the electronic structure of figure-8 electromagnetic standing waves combined with eigen-drift**, this paper establishes the formation mechanism **from figure-8 magnetic moments to electronic magnetic flux** and proposes a verifiable experimental scheme. Based on the interaction mechanism between magnetic coupling potential energy and valence electron kinetic energy, a first-order criterion for superconductivity is derived: $\boldsymbol{\Gamma = 7.285}$ eV , also known as the “golden

boundary" for superconductivity.This criterion was validated on 28 ambient-pressure elemental superconductors, with an average relative offset of $\boldsymbol{\delta = +0.52\%}$ , demonstrating good predictive performance; when used to validate non-superconducting control elements, the average relative offset was $\boldsymbol{\delta = -117.3\%}$ **, showing a significant difference between the two groups of samples and clear distinguishing features.**Unlike the traditional BCS framework, this model does not require the introduction of phonon coupling or the Cooper pairing hypothesis; instead, it explains the formation conditions of elemental superconductivity based on the balance between the kinetic energy of valence electrons and the magnetic coupling potential energy. The model is logically consistent and supported by existing atomic spectral data, providing an independent physical picture of the microscopic mechanisms of superconductivity. It holds high practical value and theoretical significance for future superconductivity research.

---

**References**


[1] Bardeen J, Cooper L N, Schrieffer J R. Theory of Superconductivity. Physical Review, 1957, 108(5): 1175–1204.

[2] McMillan W L. Transition temperature of strong-coupled superconductors. Physical Review, 1968, 167(2): 331–344.

[3] Bednorz J G, Müller K A. Possible high-Tc superconductivity in the Ba-La-Cu-O system. Zeitschrift für Physik B – Condensed Matter, 1986, 64(2): 189–193.

[4] Anderson P W. Resonating valence bonds: A new kind of insulator? Materials Research Bulletin, 1973, 8(2): 153–160.

[5] Zhao Z X. Exploration of high critical temperature superconductors. Physics (in Chinese), 1977, 6(4).

[6] Sun Z. Topology of Electronic Locks—Physical and Mathematical Models of Figure-8 Electromagnetic Standing Waves and Eigen Drift. Zenodo, 2026. https://doi.org/10.5281/zenodo.21669555.

[7] Kramida, A., Ralchenko, Y., Reader, J., & NIST ASD Team. (2024). NIST Atomic Spectra Database (Version 5.12). National Institute of Standards and Technology. https://physics.nist.gov/asd.

[8] Fock V. Bemerkung zum Virialsatz. Zeitschrift für Physik, 1930, 63(11–12): 855–858.